E213 : Analysis of Decays of heavy vector boson Z^0

A lab report written by
Group P20: Mrunmoy Jena and Ajay Shanmuga Sakthivasan

Supervisor: Martin Angelsmark

Universität Bonn
May 25, 2022

Contents

Introduction

Prerequisite Knowledge

1.1 The Standard Model- A Brief Overview

The Standard Model of particle physics which has been one of the most successful and well-tested theories so far, provides the most fundamental description of nature by incorporating the elementary particles and their interactions. These elementary particles are categorized into two families: fermions (having half integer spins) which form matter as we know it, and bosons (with integer spins) serving as mediators of the three fundamental forces. While electromagnetic interactions are mediated by the photon (γ); strong and weak interactions are mediated by gluons (g) and by $W^{\pm}, Z^{0}$ bosons respectively. A fundamental particle that mediates gravitation has been only postulated theoretically, and is left out of the Standard Model, since the effects of gravity are too weak to play any important role in the realm of particle physics.

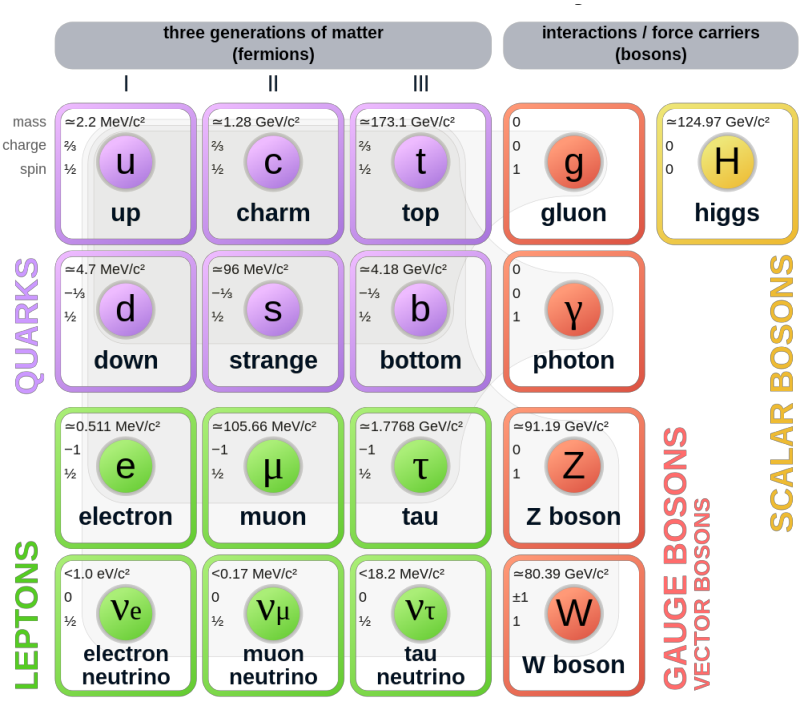

Figure 1.1: A chart showing the families of elementary particles in the Standard Model

The fermions consists of three generations of quarks and leptons. The quarks have six flavours: up (u), down (d), charm (c), strange (s), top (t) and bottom (b). Similarly, the leptons consist of the electron (e), muon (μ) and tau (τ), each having its own associated charge-less and almost massless neutrino (ν_e, ν_μ and ν_τ). Furthermore, each particle in the standard model has its own antiparticle. The quarks are able to form composite particles in either three quark combinations, called baryons ($qqq/\bar{q}\bar{q}\bar{q}$) or a quark-antiquark pair, called a meson ($q\bar{q}$). Mathematically, the elementary particles are described as elements of representations of certain symmetry groups. The gauge fields that couple to these particles (i.e. mediate the interactions) arise naturally as a consequence of invariance of their corresponding Lagrangian under

local group transformations [1]. As such, the gauge symmetry that governs the Standard Model is given by:

$$SU(3)_{\text{Colour}} \times SU(2)_{\text{Left chiral}} \times U(1)_{\text{Y(Weak hypercharge)}}$$

1.2 The Unified Theory of Electromagnetic and Weak Interactions

Since the experiment deals with verifying some of the properties of the Z^0 bosons, it is of interest to touch upon the theory of electroweak unification.

While electromagnetism and the theory of weak interactions were formulated separately, it was later on postulated that at higher energies (~ 246 GeV [2]), both these interactions would be unified into a single force. As such, the GSW(Glashow-Salam-Weinberg) electroweak model was developed in the 1960s to describe this unified force.

One finds that imposing the principle of local gauge invariance on the $SU(2)_L$ symmetry group leads to the introduction of three gauge fields: $W^{(1)}$, $W^{(2)}$ and $W^{(3)}$ (or W^0 in some references) [1]. The physical W^+ and W^- bosons (that mediate the weak charged current interaction) can be seen as the linear combinations:

$$W^{\pm} = \frac{1}{\sqrt{2}} \left(W^{(1)} \mp W^{(2)} \right) \tag{1.1}$$

However, the $W^{(3)}$ field has no physical interpretation of its own. Therefore an additional symmetry, the $U(1)_Y$ group is introduced. The field B (or equivalently Y^0) arising as a consequence of this new symmetry, similarly does not have a physical meaning on its own. Rather, it was seen that linear combinations of the $W^{(3)}$ (W^0) and B (Y^0) fields gives rise to the photon and the Z^0 boson:

$$\begin{pmatrix} \gamma \\ Z^0 \end{pmatrix} = \begin{pmatrix} \cos\theta_W & \sin\theta_W \\ -\sin\theta_W & \cos\theta_W \end{pmatrix} \begin{pmatrix} B \\ W^{(3)} \end{pmatrix} \tag{1.2}$$

where θ_W is the weak mixing/Weinberg angle

In addition to this, it is to be noted that the gauge fields $W^{(1),(2),(3)}$ and B have to be massless, in order to respect gauge invariance under local $SU(2)_L \times U(1)_Y$ gauge transformation. However, the physical gauge bosons $W^{\pm}$ and Z^0 are predicted to be massive, whereas the photon should remain massless. To explain this, the concept of electroweak spontaneous symmetry breaking was introduced. A massive scalar field (the Higgs field) is introduced, to which these bosons ($W^{\pm}$, Z^0) must couple to, in order to get their physical masses, while the photon does not interact with it [3]. The intricacies of the Higgs mechanism are not of immediate interest here, and can be understood from standard references [1, 4].

1.3 Physics Related to the Z^0 Resonance

1.3.1 e^+e^- Interactions

Before discussing the processes of interest involving Z^0 production, we first list out the important ways in which e^+e^- pairs can interact [5]:

- $\boldsymbol{e^+e^- \to e^+e^-}$: Bhaba scattering (elastic scattering) of e^+e^- pairs

- $\boldsymbol{e^+e^- \to e^+e^-\gamma\gamma}$: two photon process; e^+e^- can scatter off of virtual photons, arising out of the incoming e^- and e^+ themselves and these photons can then produce hadrons
- $\boldsymbol{e^+e^- \to f\bar{f}}$: Electron-positron pairs annihilate to produce a gauge boson (γ or Z^0), which would in turn produce a fermion-antifermion ($f\bar{f}$) pair. Here $f\bar{f}$ are fermions other than e^+e^- since that process is already included under Bhaba scattering.
- $\boldsymbol{e^+e^- \to \gamma\gamma/\gamma\gamma\gamma}$: An electron-positron pair could also produce two or three photons

These e^+e^- interactions are displayed in Figure 1.2.

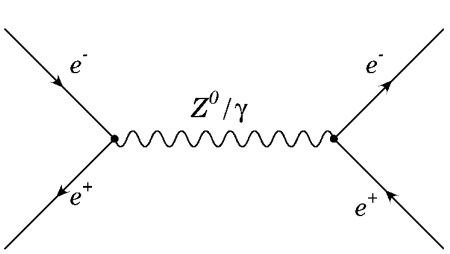

(a) s-channel Bhaba scattering

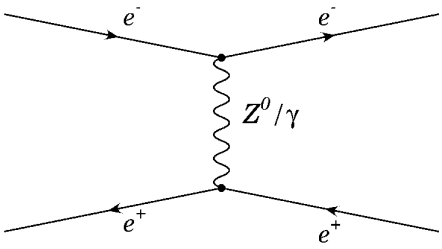

(b) t-channel Bhaba scattering

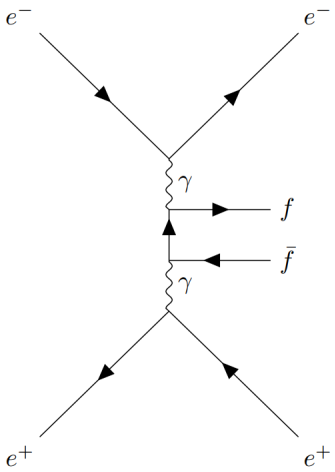

(c) Two photon process

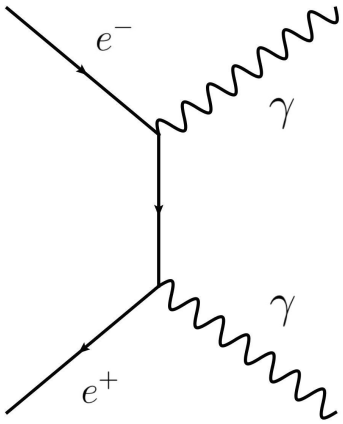

(d) Production of two photons from e^+e^- pair

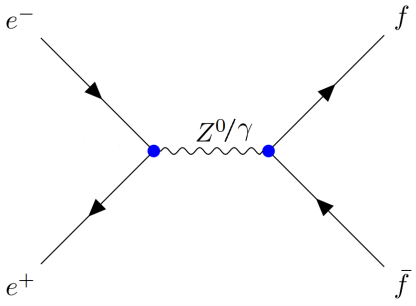

(e) Electron-positron annihilation to $f\bar{f}$

Figure 1.2: Some examples of e^+e^- interactions [5–7]

In case of the lowest order $e^+e^- \to f\bar{f}$ process, there are contributions to cross section from pure Z^0, pure γ as well as from $\gamma - Z^0$ interference terms. However, near center of mass energies close to the Z^0 resonance, the major contribution to the total cross section is from the pure Z^0 term.

Additionally, it is easy to see that for the particular case of $e^+e^- \to e^+e^-$ scattering (Bhaba scattering), there is a t-channel contribution in addition to the s-channel component. The cross sections of both these processes have have different angular dependencies [5]

$$\left(\frac{d\sigma}{d\Omega}\right)_s \propto (1 + \cos^2\theta) \tag{1.3}$$

$$\left(\frac{d\sigma}{d\Omega}\right)_t \propto (1 - \cos\theta)^{-2} \tag{1.4}$$

This means that while the s channel cross section has a major contribution at large angles (or small values of $\cos\theta$), the t-channel contribution increases asymptotically at small angles (or large values of $\cos\theta$). As shall be seen later on, removing the t-channel contribution is an essential step, since we are only concerned with finding the inherent forward-backward asymmetry associated with the s-channel processes.

1.3.2 Forward-Backward Asymmetry

When we consider the s-channel processes $e^+e^- \to f\bar{f}$, as discussed before, if the process is mediated purely by photons (γ) then the differential cross section follows the $(1+\cos^2\theta)$ dependence and it shows a symmetric dependence on the scattering angle θ. However, for the same process mediated by Z^0 bosons we find that there is an additional term contributing to the asymmetry:

$$\left(\frac{d\sigma}{d\Omega}\right)_{s\ (Z^0)} \propto a(1 + \cos^2\theta) + 2b\cos\theta \tag{1.5}$$

From theory of electroweak interactions, this asymmetry (between the number of fermions produced in the forward direction, $\theta > \pi/2$ and the backward direction, $\theta < \pi/2$) can be understood to be arising from the fact that the Z^0 does not couple equally to right handed and left handed fermions. This becomes more clear by looking at the form of the asymmetry term:

$$b = \left[(g_L^e)^2 - (g_R^e)^2\right]\left[\left(g_L^f\right)^2 - \left(g_R^f\right)^2\right] \tag{1.6}$$

where g_L^f and g_R^f signify the coupling of Z^0 to left handed and right handed fermions respectively. It can be clearly seen that in case the these two couplings had been equal, the asymmetry term would have gone to zero [1].

The forward backward asymmetry factor is given as the ratio:

$$\mathcal{A}_{fb} = \frac{\sigma_F - \sigma_B}{\sigma_F - \sigma_B} = \frac{3b}{4a} \tag{1.7}$$

where σ_F and σ_B are the cross sections in forward and backward directions respectively.

It is found that at the resonance of Z^0 boson, $\mathcal{A}_{fb}$ simplifies to [5]:

$$\mathcal{A}_{fb}^{f} \approx 3 \left(\frac{g_V^f}{g_A^f} \right) = 1 - 4 \sin^2 \theta_W \tag{1.8}$$

Thus from the calculation of the forward-backward asymmetry, the ratio of g_V^f (vector coupling strength between Z^0 and fermions) to g_A^f (axial vector coupling strength between Z^0 and fermions) can be found, which in turn gives us the Weinberg (weak mixing) angle θ_W.

1.3.3 Background Processes: Radiative Corrections

In order to test out the predictions of the Standard Model at a very high level of precision, higher order background processes need to be accounted for and as such the corrections made due to these processes are called 'radiative corrections'. The following are some of these processes that need to be accounted for [8]:

- **Initial state radiation (ISR):** The radiation of photons in the initial state lead to decrease in the centre of mass energy and thus affect the Z^0 resonance peak parameters. This leads to a peak height reduction by upto 25 %, shift of peak to higher energy and increase in full width at half maximum (FWHM).
- **Final state radiation (FSR):** When photons or gluons are radiated in the final state, it is found that partial widths increase by the corresponding factors:

$$\Delta_{QED} = 1 + \frac{3}{4} \frac{Q_f^2 \alpha(m_Z^2)}{\pi} \; ; \; \Delta_{QCD} \approx 1 + \frac{\alpha_s(m_Z^2)}{\pi} \tag{1.9}$$

- **QED vacuum polarization:** The production of e^+e^- pairs from vacuum makes the QED coupling constant scale dependent:

$$\alpha(s) = \frac{\alpha_0}{1 - \Delta\alpha(s)} \tag{1.10}$$

  It has been shown that the imaginary part of $\Delta\alpha(s)$ has an influence on the γ/Z^0 interference term.

- **Electroweak corrections:** Further contributions also arise from virtual processes such as higher order loops in Z^0 propagator and vertex corrections.

  Some instances of these radiative corrections are shown in Figure 1.3

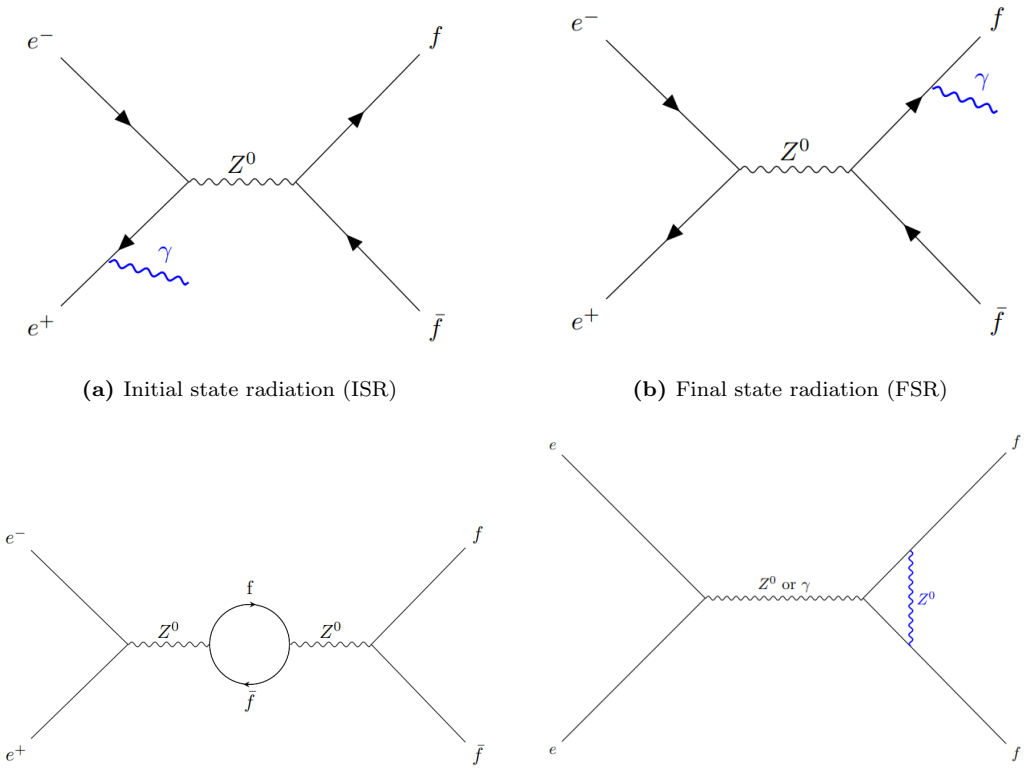

(a) Initial state radiation (ISR)

(b) Final state radiation (FSR)

(c) Z^0 propagator correction

(d) Z^0 vertex correction

Figure 1.3: Some examples of radiative corrections [5]

1.3.4 Important Parameters of a Resonance Particle

1.4 High Energy Colliders

The Large Electron Positron Collider (LEP) was built at CERN, with one of its major goals being making high precision measurements of the parameters of the Z^0 boson, such as its mass, decay width and angular distributions of final state particles produced from Z^0 decays. As such, for most of its period of operation from 1989 to 1995, it produced e^+e^- collisions at centre of mass energies very close to the Z^0 resonance and about 17 million $e^+e^- \rightarrow Z^0$ events were recorded in this time frame [1]. It was built in such a manner that the electron-positron collisions took place at four different points in the circular collider, and hence four such detectors were used in this experiment: ALEPH (Apparatus for LEP PHysics), DELPHI (DEtector with Lepton, Photon and Hadron Identification), L3 (Third LEP experiment) and OPAL (Omni-Purpose Apparatus for LEP).

The components of the OPAL detector shall be described in further detail in this Section, since this experiment focuses on analysis of data collected by the OPAL.

1.4.1 The OPAL Detector

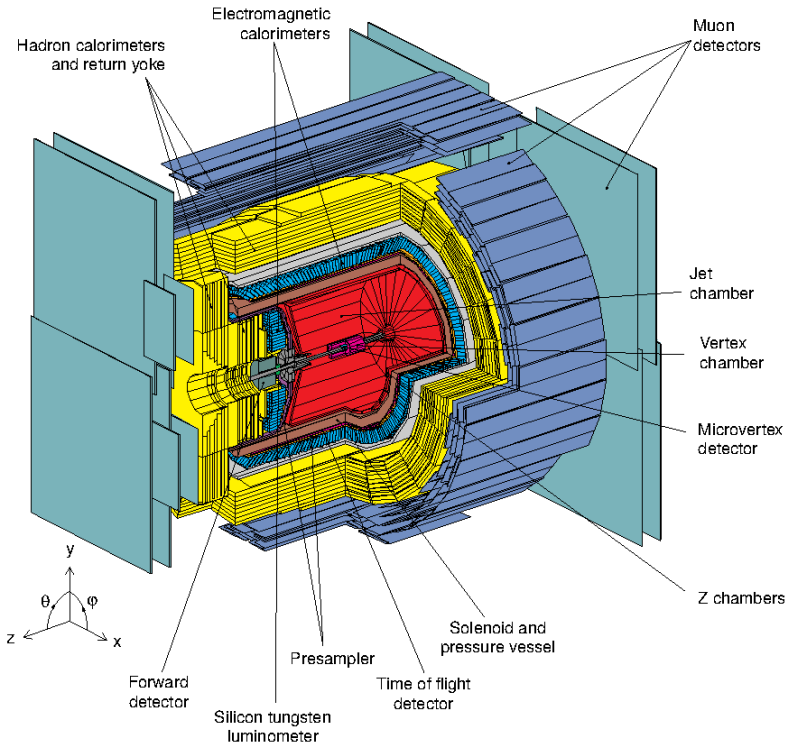

Figure 1.4: The OPAL Detector and its various components

For analysis of events arising from this detector, a right handed coordinate system is followed. The origin is fixed at the point where e^+e^- collisions take place, the x axis points horizontally in the direction of the center of the LEP, while the z axis is defined to lie along along the beam path and the y axis is then just perpendicular to the $x-y$ plane as usual. θ, the polar angle is the angle between the y and z axes and the azimuthal angle ϕ is the counterclockwise angle between the x and y directions. The OPAL detector and this coordinate system is displayed in Figure 1.4.

Starting from the origin, as the e^+e^- collision products fly outwards, various detector components are encountered which serve to detect the type and various characteristics of the final state particles. These primary detector components are discussed here in brief:

- **Vertex detector:** This is a type of drift detector that surrounds the central beam pipe and plays a key role in locating vertices of short-lived decay products and also helps in improving the momentum resolution. It has dimensions of 1 m in length and measures 470 mm across (diameter), layered with 36 axial cells that measure positions in the $r-\phi$ plane.
- **Jet chamber:** This is again a cylindrical drift chamber with a good spatial and track resolution, designed in a manner so as to efficiently record events associated with jets. Inside this chamber, there are 24 sectors, each of which contains 159 sensing wires, arranged parallel to the beam axis. Beside the anode wires, there are alternating potential wires and cathode wires positioned in between the potential and anode wires. The coordinates of the decay particles are obtained from

parameters such as the positions of the wires and the drift time. Moreover, the signals from these wires determine the energy loss dE/dx of charged particles in this region.

- **z chambers:**
- **Time of flight (TOF) system:**
- **Electromagnetic calorimeter (ECAL):**
- **Hadron calorimeter (HCAL):**
- **Muon detector:**

Pre-Lab Exercises

In this chapter, we have provided our solutions to some theoretical questions that were needed to be solved before conducting the experiment. All the equations and standard values of parameters used to calculate the numerical results for these exercises are taken from [5], unless mentioned otherwise.

2.1 Calculation of partial decay widths for $Z^0 \to f\bar{f}$

In this exercise, we are required to calculate the partial decay widths of $Z^0 \to f\bar{f}$; where $f\bar{f}$ represent the following fermion-antifermion pairs : (i) e^+e^- (ii) $\mu^+\mu^-$ (iii) $\tau^+\tau^-$ (iv) $q\bar{q}$, where q represents all the flavours of quarks (except for t quark, because it is too heavy ($M_t \approx 172.76$ GeV [9]) to be produced from Z^0 decays). The partial decay widths have been calculated with the following formula:

$$\Gamma_f = \frac{N_c^f \sqrt{2}}{12\pi} G_F M_Z^3 \left(\left(g_V^f\right)^2 + \left(g_A^f\right)^2 \right) \tag{2.1}$$

where:

N_c^f: colour factor, (1 for leptons, 3 for quarks)

$G_F = 1.16637 \times 10^{-5}\text{GeV}^{-2}$, Fermi's constant

$M_Z = 91.182$ GeV, mass of Z^0 boson

$g_V^f = I_3^f - 2Q_f \sin^2\theta_W$, vector coupling strength of Z^0 to fermions

$g_A^f = I_3^f$, axial-vector coupling strength of Z^0 to fermions

Q_f: electric charge of fermion f

I_3: third component of weak isospin

$\sin^2\theta_W = 0.2312$, θ_W is the Weinberg (weak-mixing) angle

Fermion	$\mathbf{Q_f}$	$\mathbf{I_3^f}$	$\mathbf{g_V^f}$	$\mathbf{g_A^f}$	$\mathbf{N_c^f}$	$\mathbf{\Gamma_f^{(calc)}}$ **/MeV**	$\mathbf{\Gamma_f^{(ref)}}$ **/MeV**
e^-, μ^-, τ^-	-1	-0.5	-0.0376	-0.5	1	83.89	83.8
u, c	2/3	0.5	0.1917	0.5	3	285.34	299
d, b, s	-1/3	-0.5	-0.3459	-0.5	3	367.84	378
ν_e, ν_μ, ν_τ	0	0.5	0.5	0.5	1	165.85	167.6

Table 2.1: Parameters $Q_f, I_3^f, g_V^f, g_A^f, N_c^f$ for various fermion pairs and their partial decay widths

The calculated partial decay widths for the required fermion pairs have been listed under $\Gamma_f^{(calc)}$ in Table 2.1. Further, the reference [5] values of partial decay widths for the same fermion pairs are listed under $\Gamma_f^{(ref)}$ for comparison. We have also included the partial decay widths of the three neutrinos since they would be used in the solution to the next exercise.

One finds that calculated values of partial decay width for the lepton pairs are in close agreement with the literature value, deviating by about 0.1% to 1%. The slight deviation could be caused because the

$\gamma \to f\bar{f}$ term and interference terms have been neglected. In case of the quarks, the deviations from the reference values are higher ($\sim$ 2.7% to 4.6%). This may be due to the fact that additionally, the effect of strong interactions have not been accounted for in our calculations.

2.2 Calculation of hadronic, leptonic and total decay widths and cross section

Hadronic decay width: The decay widths for the hadronic mode is given by the sum of the partial decay widths of the u,d,c,s and b quarks:

$$\Gamma_{had} = \Gamma_u + \Gamma_c + \Gamma_d + \Gamma_s + \Gamma_b = 2 \cdot \Gamma_{u,c} + 3 \cdot \Gamma_{d,s,b} = 1674.20 \text{ MeV}$$

'Charged' decay width: The charged leptons, e, μ, τ will contribute to this decay width:

$$\Gamma_{charged\ leptonic} = \Gamma_e + \Gamma_\mu + \Gamma_\tau = 3 \cdot \Gamma_{e,\mu,\tau} = 250.17 \text{ MeV}$$

'Neutral' (invisible) decay width: The uncharged leptons ($\nu_e,\ \nu_\mu,\ \nu_\tau$) will contribute to this:

$$\Gamma_{neutral\ leptonic} = \Gamma_{\nu_e} + \Gamma_{\nu_\mu} + \Gamma_{\nu_\tau} = 3 \cdot \Gamma_{\nu_e} = 497.55 \text{ MeV}$$

Total Z^0 decay width: The total decay width for Z^0 will just be the sum of the hadronic, charged leptonic and neutral leptonic decay widths:

$$\Gamma_{total} = \Gamma_{hadronic} + \Gamma_{charged\ leptonic} + \Gamma_{neutral\ leptonic} = 2421.92 \text{ MeV}$$

Partial cross sections at maximum of resonance: At resonance, the formula for calculating partial cross section for $Z^0 \to f\bar{f}$ becomes:

$$\sigma_f^{peak} = \frac{12\pi\Gamma_e\Gamma_f}{M_Z^2\Gamma_Z^2} \tag{2.2}$$

The calculated partial cross sections for the different decay channels along with the respective decay widths are tabulated in Table 2.2.

Decay channel	**Decay width / MeV**	**Partial cross section / 10^{-11} MeV^{-2}**
Hadronic (u,d,c,s,b)	1674.20	10.79
Charged leptonic (e, μ, τ)	250.17	1.61
Neutral leptonic ($\nu_e,\ \nu_\mu, \nu_\tau$)	497.55	3.21
Total	2491.92	15.61

Table 2.2: Calculated decay widths and partial cross sections for different Z^0 decay channels

2.3 Effect of additional generation on width of Z^0 resonance curve

In case it is possible for the Z^0 to decay into an extra generation of light fermions (u,d,e,ν), the total decay width will increase, and the new total decay width will be:

$$\Gamma_{total}^{(new)} = \Gamma_{total} + \Gamma_e + \Gamma_\nu + \Gamma_u + \Gamma_d = 3324.34 \text{ MeV}$$

The percentage increase in the width of the Z^0 resonance curve will be:

$$\frac{\Gamma_{total}^{(new)} - \Gamma_{total}}{\Gamma_{total}} = \frac{902.42}{2421.92} \times 100\% = 37.26\%$$

2.4 Angular distributions of differential cross sections

On studying the dependence of differential cross sections of e^+e^- processes on the azimuthal angle θ, it is found that the s-channel has a symmetrical dependence on θ (with an additional small asymmetric term, in the case of Z^0 mediated process; which will be calculated later):

$$\left(\frac{d\sigma}{d\Omega}\right)_s \propto \left(1 + \cos^2\theta\right) \tag{2.3}$$

For the case of a t-channel process, it is found that the differential cross section diverges quickly at small θ values [5]:

$$\left(\frac{d\sigma}{d\Omega}\right)_t \propto \left(1 - \cos\theta\right)^{-2} \tag{2.4}$$

While the process $e^+e^- \to \mu^-\mu^+$ can only take place through the s-channel; the $e^+e^- \to e^+e^-$ process can occur through both s and t channels. The angular distributions of these two processes are shown in Figure 2.1. For the $e^+e^- \to e^+e^-$ process, the contributions from the s and t channels are shown separately as well as their combined contribution to the differential cross section.

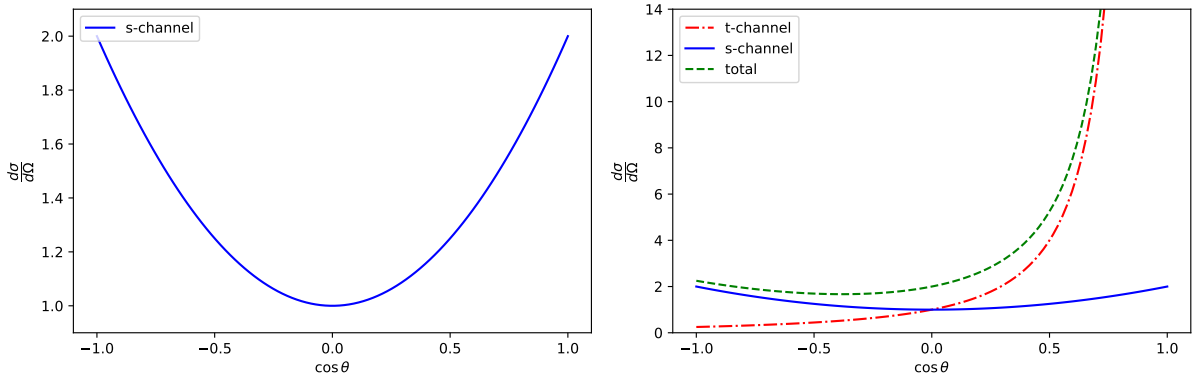

Figure 2.1: Angular distributions of $e^+e^- \to \mu^+\mu^-$ (left) and $e^+e^- \to \mu^+\mu^-$ (right)

2.5 Calculation of forward-backward asymmetry

We are required to calculate the forward-backward asymmetry factor, A_{FB} in the process $e^+e^- \to \mu^+\mu^-$. In order to do this, the following formula is used:

$$A_{FB} = \frac{3F_2}{4F_1} \tag{2.5}$$

where the parameters are given by:

$F_1(s) = Q_f^2 - 2v_e v_f Q_f \mathfrak{Re}(\chi) + (v_e^2 + a_e^2)(v_f^2 + a_f^2)|\chi|^2$

$F_1(s) = -2a_e a_f Q_f \mathfrak{Re}(\chi) + 4v_e a_e v_f a_f |\chi|^2$

$v_f = \dfrac{g_V^f}{2\sin\theta_W \cos\theta_W}$

$a_f = \dfrac{g_A}{2\sin\theta_W \cos\theta_W}$

$\chi(s) = \dfrac{s}{\left((s - M_Z^2) + is\dfrac{\Gamma_Z}{M_Z}\right)}$, Propagator

s: Square of centre-of-mass energy

$\sin^2\theta_W$ \ $\sqrt{s}$ / GeV	89.225	91.225	93.225
0.21	-0.0937	0.0762	0.2317
0.23	-0.1639	0.0228	0.1965
0.25	-0.1948	0.0042	0.1906

Table 2.3: Forward backward asymmetry factors for different Weinberg angles (θ_W) and centre of mass energies ($\sqrt{s}$)

Analysis

3.1 Part I: Analysis of Event Displays

The first part of the analysis of data consists of looking at event displays, which are generated using *GRope*. The main objective of this part is to understand how different channels affect different observed quantities and how we can come up with a filter to the quantities, so as to separate out different channels in a real world data. The filters are known as the cut criteria for this process. Every event display consists of an image and a list of quantities,

- Ctrk(N): Number of charged tracks
- Ctrk(Sump): Momentum of all charged tracks
- Ecal(SumE): Total energy in the electromagnetic calorimeter
- Hcal(sumE): Total energy in the hadronic calorimeter

We have eight different samples for this part - four *pure* samples and four *mixed* samples. Each of the four *pure* samples consists of only the events from a single channel, whereas the four *mixed* samples consists of events from all the channels. We would analyse *pure* samples first and come up with a cut criteria and test it on the *mixed* samples and see how it fares.

3.1.1 Analysis of e^-e^+-channel Samples

The decay of Z^0 boson into an electron-positron pair is one of the channels of this process. For this case, we expect to detect two charged tracks. Since the pair has negligible mass compared to Z^0 boson, they carry away the center of mass energy, which implies *SumP* will have this value. By construction of the detectors, we expect all the energy to be deposited in the electromagnetic calorimeter, while the signals should be close to zero in other components. The event display of a typical event can be found in B.1, which shows two clear charged tracks and also shows that they deposit their energy in the electromagnetic calorimeter. By conservation of four-momenta, we should also expect to see the tracks exactly opposite to each other, which can also be seen here.

3.1.2 Analysis of $\mu^-\mu^+$-channel Samples

The decay of Z^0 boson into an muon-antimuon pair is another channel of this process. Just like the previous case, we expect to see two charged tracks and *SumP* value being close to the center of mass energy value. By construction of the detectors, we expect close to zero energy deposit in the calorimeters. But instead, we expect to see a signal in the muon chambers. The event display of a typical event can be found in B.2, which shows two clear charged charged tracks and signals in the muon chamber. We also see that conservation of four-momenta holds, since the tracks are exactly opposite to one another.

3.1.3 Analysis of $\tau^-\tau^+$-channel Samples

The decay of Z^0 boson into an tau-antitau pair is another channel of this process. Unlike its other leptonic cousins, τ has a much shorter life, which results in interesting outcomes here. We expect to see a large number of charged tracks due to the decay, clustered exactly opposite to each other due to conservation of four-momenta. The dominant decay products are μ and π, which can then be detected in the other components of the detectors. This channel can be classified by the number of charge tracks, called *prongs*. The event display of a *3-prong* event can be found in B.3. We can see the signals in muon chamber on one side and we can also see the deposit in electromagnetic calorimeter and hadronic calorimeter on the other side, which corresponds to the pions. We should also expect the *SumP* value to be less than the center of mass energy, since neutrinos are produced to conserve lepton number, which carry away some of the energy. Unlike the previous two cases, this channel doesn't have a very distinct filter property at the first sight.

3.1.4 Analysis of $q\bar{q}$-channel Samples

The decay of Z^0 boson into an quark-antiquark pair is another channel of this process. Since quarks cannot exist as free particles, they produce hadrons, which then decay into further particles that can be then detected at various components. This results in the so-called *jets*, which are much bigger clusters of charged tracks. Depending on the final products, we expect to notice signals in all of the components of the detectors. But one distinct property of this channel is the large number of charged tracks produced. The event display of a typical event can be found in B.4, which clearly shows the jets. Again, we expect the *SumP* value to be lesser than center of mass energy, since depending on the decay products, various neutrinos are produced to conserve lepton number, which carry away some of the energy.

3.2 Part II: Statistical Analysis of Z^0 Decays

In the previous subsection, we carried out an analysis based on event displays. This was possible because we did not have a lot of events to work with. Obviously, such an analysis would prove to be futile if we try to carry it out on a large set of data. Analysis of large sets of data would be the primary discussion of this subsection. We use the software, *ROOT* to analyse the data on a statistical basis. *ROOT* works with *.root* files, which contain all the information in a tree-like structure, called *ntuple*. The contents of the *ntuple* are,

- RUN: Run number
- EVENT: Event number
- NCHARGED: Number of charged tracks
- PCHARGED: Total scalar sum of track momenta
- E_ECAL: Total energy in electromagnetic calorimeter
- E_HCAL: Total energy in hadronic calorimeter
- E_LEP: LEP beam energy ($= \sqrt{s}/2$)
- COS_THRU: cos(polar angle) between beam axis and thrust axis

- COS_THET: cos(polar angle) between incoming positron and outgoing positive particle

We also have two categories of data, each containing a lot of *ntuples*,

- Monte Carlo (MC): These correspond to the "*pure*" events from the previous subsection. These are simulated - detector response to a calculated outgoing momentum four-vector for a specific process.
- Data: These correspond to the "*mixed*" events from the previous subsection. These are real life data recorded with the OPAL detector at specific energies around the Z^0 resonance maximum.

ROOT can be used to set cuts on the above variables in a data and get histograms of different variables. This allows for a statistical analysis of the data. All the above information can be found in [5].

3.2.1 Refining the cuts

As mentioned previously, we have two categories of data. There are four Monte Carlo (MC) data, one for each of the decay channels. There are six real world data and we will be using *data6.root* for our analysis in the following parts. Analysis of event displays already gave us an idea of what cuts to use, to extract the different channels. Our first step here will be to test our cuts on the MC data and check how they fare. And the second step will be to refine the cuts a little so that we are better able to extract different channels.

When it comes to e^-e^+ final state decay channel, we would like to exclude t-channel events. This is because t-channel is possible only in the mode and for the sake of consistency, we would like to limit ourselves to only s-channel. From theory[5], we know that the t-channel dominates at large $cos\theta$. By introducing a new cut to exclude events with large $cos\theta$, we eliminate a most of the t-channel events. But this also means that we are eliminating some of the s-channel events. To account for this, we multiply the observed events after applying the modified cuts with correction factor. This correction factor is given by,

$$\delta = \frac{\int_{-1}^{1}(1+x^2)dx}{\int_{-0.9}^{0.5}(1+x^2)dx} \approx 1.5829. \tag{3.1}$$

This factor is arrived at from theory, which gives the behaviour of s-channel as proportional to $(1+cos^2\theta)$ and the integral limits are correspond to the $cos\theta$ values which we exclude.

When it comes to $\mu^-\mu^+$ final state decay channel, we observed a lot of events with $PCHARGED$ equal to exactly 0. These events are not physical. Hence we apply a cut to eliminate such events. In the cases of e^-e^+ and $\mu^-\mu^+$, we also exclude $cos\theta$ values very close to 1 and -1, as the detector resolution is far from perfect close to the beam axis. To summarise, we have the following additions - $cos\theta \in [-0.9, 0.5]$, to remove t-channel events in the case of e^-e^+, $PCHARGED > 0$, to exclude unphysical events in the case of e^-e^+ and $cos\theta \in [-0.9, 0.9]$, to eliminate low resolution events in the cases of e^-e^+ and $\mu^-\mu^+$. Interestingly, the channels $\tau^-\tau^+$ and $q\bar{q}$ did not require any additional global cuts. But, we did add the cut $cos\theta \in [-1, 1]$ to remove any unphysical events. Analysis done with $ROOT$ on the e^-e^+ MC can be found in the appendix, B.5, B.6, B.7, B.8 and B.9. Analysis on the other MC files and ultimately the data file are done similarly.

After testing our cuts, we arrive at the conclusion that we don't need any further refinements other than the additions mentioned above. With these additions, we go about analysing *data6.root*. The raw data of observed events using our cuts is given in the table 3.1 below. Note that the correction factor has not been applied to the e^-e^+ event numbers but it is used in our latter calculations. The event numbers are

exactly what we get after applying all the cuts appropriately.

	Number of observed events				
MC Sample	e^-e^+ cuts	$\mu^-\mu^+$ cuts	$\tau^-\tau^+$ cuts	$q\bar{q}$ cuts	Total (incl. global cuts, if any)
e^-e^+	18835	0	378	0	56720
$\mu^-\mu^+$	0	76209	8599	0	89887
$\tau^-\tau^+$	26	35	71131	135	79214
$q\bar{q}$	0	0	173	92164	98563

Table 3.1: Number of events with different cuts applied to each of the MC data.

3.2.2 Efficiency Matrix

The efficiency matrix is a measure of how efficient the cuts are at extracting the different decay channels. If we consider the actual event numbers of the different channels as a 4×1 matrix, the efficiency matrix will be a 4×4 matrix and ideally, it should be a unit matrix. In this case, the event numbers observed matches the actual event numbers. But this is not the case usually. We should aim to achieve an efficiency matrix with diagonal elements as close to 1 as possible and the off-diagonal elements as close to 0 as possible. The efficiency matrix elements are given by[5],

$$\epsilon_{ij} = \frac{N_j^{i,cut}}{N_j^{j,all}}. \tag{3.2}$$

For example, ϵ_{12} corresponds to e^-e^+ cuts applied to $\mu^-\mu^+$ events divided by the total observed $\mu^-\mu^+$ events. Note that we construct the 4×1 matrix in the following order - e^-e^+ events, $\mu^-\mu^+$ events, $\tau^-\tau+$ events and $q\bar{q}$ events. With this efficiency matrix, one could extract the actual event numbers as follows,

$$N_{obs} = \epsilon N_{actual} \implies N_{actual} = \epsilon^{-1} N_{obs}. \tag{3.3}$$

This gives us an efficiency matrix,

$$\epsilon = \begin{pmatrix} 5.26 \times 10^{-1} & 0 & 3.28 \times 10^{-4} & 0 \\ 0 & 8.48 \times 10^{-1} & 4.42 \times 10^{-4} & 0 \\ 6.66 \times 10^{-3} & 9.57 \times 10^{-2} & 8.98 \times 10^{-1} & 1.76 \times 10^{-3} \\ 0 & 0 & 1.70 \times 10^{-3} & 9.35 \times 10^{-1} \end{pmatrix}. \tag{3.4}$$

Given a cut, whether or not a particular event passes it can be modelled with a binomial distribution, just like modelling a coin toss. In the limit when such an "experiment" is conducted on large sample size, the probability mass function of the binomial distribution can be approximated by a normal distribution. In which case, the standard deviation is given by,

$$\Delta\epsilon_{ij} = \sqrt{\frac{\epsilon_{ij}(1-\epsilon_{ij})}{N}}, \tag{3.5}$$

where ϵ_{ij} is a particular element of the efficiency matrix and N is the total events corresponding to that matrix element. The above treatment can be found in any introductory book on probability theory, for

example Feller[10]. This gives us the standard deviation in the efficiency matrix elements,

$$\Delta\epsilon = \begin{pmatrix} 2.10\times10^{-3} & 0 & 6.44\times10^{-5} & 0 \\ 0 & 1.12\times10^{-3} & 7.47\times10^{-5} & 0 \\ 3.41\times10^{-4} & 9.81\times10^{-4} & 1.08\times10^{-3} & 1.33\times10^{-4} \\ 0 & 0 & 1.46\times10^{-4} & 7.85\times10^{-5} \end{pmatrix}. \tag{3.6}$$

For our calculations in the following sections, we require N_{actual}. Therefore, we invert the matrix. The calculations for error in the inverse matrix elements is not straightforward. We refer to [11], which gives the error in the inverse matrix element to be,

$$(\Delta\epsilon^{-1})^2_{ij} = \sum_{\alpha=1}^{4}\sum_{\beta=1}^{4}(\epsilon^{-1})^2_{i\alpha}(\Delta\epsilon)^2_{\alpha\beta}(\epsilon^{-1})^2_{\beta j}. \tag{3.7}$$

With this we get the following inverse efficiency matrix and the error in the inverse efficiency matrix elements,

$$\begin{aligned}\epsilon^{-1} = &\begin{pmatrix} 1.90 & 7.85\times10^{-5} & -6.95\times10^{-4} & 1.30\times10^{-6} \\ 7.36\times10^{-6} & 1.18 & -5.80\times10^{-4} & 1.09\times10^{-6} \\ -1.41\times10^{-2} & -1.26\times10^{-1} & 1.11 & -2.09\times10^{-3} \\ 2.57\times10^{-5} & 2.29\times10^{-4} & -2.03\times10^{-3} & 1.07 \end{pmatrix} \pm \\ &\begin{pmatrix} 7.59\times10^{-3} & 1.54\times10^{-5} & 1.36\times10^{-4} & 2.75\times10^{-7} \\ 1.30\times10^{-6} & 1.67\times10^{-3} & 9.81\times10^{-5} & 2.02\times10^{-7} \\ 7.26\times10^{-4} & 1.31\times10^{-3} & 1.33\times10^{-3} & 1.59\times10^{-4} \\ 2.58\times10^{-6} & 1.98\times10^{-5} & 1.75\times10^{-4} & 8.98\times10^{-4} \end{pmatrix}\end{aligned} \tag{3.8}$$

3.2.3 Cross Sections

With the above inverse efficiency matrix, we can now calculate the actual event numbers and hence, the cross sections corresponding to different modes. The actual event numbers, N_{actual}, will simply be $\epsilon^{-1}N_{obs}$, as explained earlier. The error in actual event numbers is then,

$$\Delta N_{obs,i} = \sqrt{\sum_{j=1}^{4} N^2_{obs,j}(\Delta\epsilon^{-1}_{ij})^2 + \sum_{j=1}^{4}(\epsilon^{-1}_{ij})^2 N_{obs,j}}. \tag{3.9}$$

The events are assumed to obey Poisson statistics and hence, ΔN_{obs} is taken as $\sqrt{N_obs}$. With the actual event numbers, we can calculate the cross section as,

$$\sigma = \frac{N_{actual}}{\int \mathcal{L}dt} + \text{cf(radiation)}, \tag{3.10}$$

with the errors,

$$\Delta\sigma = \sqrt{\frac{(\Delta N_{actual})^2}{(\int \mathcal{L}dt)^2} + \frac{N^2_{actual}(\Delta\int \mathcal{L}dt)^2}{(\int \mathcal{L}dt)^4}}. \tag{3.11}$$

where $\int \mathcal{L}dt$ is the integrated luminosity and cf(radiation is the radiative correction factors. We use the integrated luminosity values and the radiative correction factors from from [5]. The actual event

numbers, integrated luminosity values and the radiative correction factor can be found in the tables A.6, A.7 in the appendix and the calculated cross sections for different $\sqrt{s}$ values can be found in the table 3.2.

$\sqrt{s}$ [GeV]	σ_{ee} [nb]	σ_{mm} [nb]	σ_{tt} [nb]	σ_{qq} [nb]
88.47	0.39 ± 0.03	0.30 ± 0.02	0.47 ± 0.03	7.19 ± 0.10
89.46	0.82 ± 0.04	0.65 ± 0.03	0.72 ± 0.03	14.20 ± 0.14
90.22	1.26 ± 0.04	1.16 ± 0.03	1.12 ± 0.03	25.70 ± 0.21
91.22	1.69 ± 0.02	1.82 ± 0.02	1.75 ± 0.02	40.75 ± 0.22
91.97	1.12 ± 0.05	1.32 ± 0.04	1.21 ± 0.04	28.96 ± 0.27
92.96	0.45 ± 0.04	0.55 ± 0.03	0.66 ± 0.04	13.67 ± 0.20
93.71	0.28 ± 0.03	0.34 ± 0.02	0.40 ± 0.03	8.20 ± 0.13

Table 3.2: Calculated cross section values for different $\sqrt{s}$ values.

3.2.4 Forward Backward Asymmetry and Weak mixing angle

The Z^0 boson couples differently to left- and right-handed fermions. This leads to an asymmetry in the angular distribution of final state particles. This asymmetry depends, not very surprisingly, on the weak mixing (or Weinberg) angle[1]. Therefore, by calculating this asymmetry between the forward and backward scattering particle, we can measure the weak mixing angle. We consider the $\mu^-\mu^+$ decay channel as we don't have the problem of t-channel like in the e^-e^+ decay mode. We also get two clear tracks in the case of $\mu^-\mu^+$ decay mode. We can calculate the asymmetry by measure the event numbers for $cos\theta > 0$ and $cos\theta < 0$. The forward backward asymmetry then is,

$$A_{fb} = \frac{N_+ - N_-}{N_+ + N_-} + \mathrm{cf}(A_{fb}), \tag{3.12}$$

where N_+ is the event numbers with $cos\theta > 0$ and N_- is the event numbers with $cos\theta < 0$, cf(A_{fb}) is the A_{fb} correction factor, which can be found in the table A.7. The error in A_{fb} is given by,

$$\Delta A_{fb} = \sqrt{N_- \left(\frac{2N_+}{(N_+ + N_-)^2}\right)^2 + N_+ \left(\frac{2N_-}{(N_+ + N_-)^2}\right)^2}. \tag{3.13}$$

The calculated A_{fb} can be found in table 3.3.

With this, we can calculate the weak mixing angle. For the data events, we consider the A_{fb} value at

$\sqrt{s}$ [GeV]	N_+	N_-	A_{fb}
	$\mu^-\mu^+$ data		
88.47	51	69	-0.128 ± 0.090
89.46	148	156	-0.007 ± 0.057
90.22	272	319	-0.063 ± 0.041
91.22	4297	4384	0.008 ± 0.011
91.97	387	380	0.039 ± 0.036
92.96	173	123	0.231 ± 0.057
93.71	189	150	0.209 ± 0.054
	$\mu^-\mu^+$ MC		
91.22	37807	38402	0.010 ± 0.014

Table 3.3: Forward and Backward event numbers for $\mu^-\mu^+$ mode data and MC events with the calculated A_{fb} values.

Z^0 resonance energy and calculate the weak mixing angle as,

$$sin^2\theta_W = 0.2369 \pm 0.0085, \tag{3.14}$$

and for the MC event, we calculate the weak mixing angle as,

$$sin^2\theta_W = 0.2352 \pm 0.0098. \tag{3.15}$$

The literature value for weak-mixing angle is $sin^2\theta_W = 0.23122 \pm 0.00003$ [2]. This value is within one standard deviation of both the results calculated with the $\mu^-\mu^+$ MC and the data file.

3.2.5 Lepton Universality

Lepton universality states that, since the masses of leptons are much smaller compared to that of the Z^0 boson, the cross section of all the three leptonic decay modes must be the same, at Z^0 resonance. From the table 3.2, we can see that at Z^0 resonance ($= 91.22GeV$),

$$\begin{aligned} \sigma_e &= 1.69 \pm 0.02 \text{ nb} \\ \sigma_\mu &= 1.82 \pm 0.02 \text{ nb} \\ \sigma_\tau &= 1.75 \pm 0.02 \text{ nb} \end{aligned} \tag{3.16}$$

We see that even though the values are almost equal, they are not exactly equal. The theoretical value calculated with values from [5] gives $\sigma_f = 1.99nb$. We see that the values calculated from the data are several standard deviations away from the theoretical value, even though they match up to the order and in fact, quite close. We postulate that this is due to the fact that we don't have the best possible cut criteria. That is, we are undercounting the event numbers to some extent, which results in the lower cross section values. And since the factor by which we undercount differs between different modes, we get cross sections that slightly differ from each other. This problem could be overcome by substantially increasing the number of events. We calculate the ratios of the hadronic to the leptonic modes as follow,

$$\begin{aligned} \frac{\sigma_{had}}{\sigma_e} &= 24.18 \pm 0.30 \\ \frac{\sigma_{had}}{\sigma_\mu} &= 22.43 \pm 0.24 \\ \frac{\sigma_{had}}{\sigma_\tau} &= 23.28 \pm 0.26 \end{aligned} \tag{3.17}$$

The ratios above directly reflect the deviations we had in the cross section values and a little greater than the theoretical value. The literature values are given by $\frac{\sigma_{had}}{\sigma_e} = 20.804 \pm 0.050$, $\frac{\sigma_{had}}{\sigma_\mu} = 20.785 \pm 0.033$ and $\frac{\sigma_{had}}{\sigma_\tau} = 20.764 \pm 0.045$ respectively [12]. Again, we are several orders of standard deviation away. But, both they are of the same order of magnitude and comparable. This means that the problem in our data is not fundamental and could be overcome by improving our counts.

3.2.6 Breit-Wigner Fit of Cross Section

Now we extract the all important quantities from our data. To do this, we fit our cross section values against a Breit-Wigner curve of the form,

$$\sigma_f(s) = \frac{12\pi}{M_Z^2} \frac{s\Gamma_e\Gamma_f}{(s - M_Z^2)^2 + \left(\frac{s\Gamma_Z}{M_Z}\right)^2} (\hbar^2 c^2), \tag{3.18}$$

which has three parameters, M_Z, Γ_Z and $\Gamma_e\Gamma_f$. The factor $\hbar^2 c^2 = 3.893793719 \times 10^5$nb GeV^2 is used to convert the cross section values to SI units from natural units. We used *scipy.optimize* module for *Python* to fit the function against our data. The plots are given in 3.1. The fit parameters obtained along with the reduced χ^2 values for the fit can be found in the table 3.4.

We have three parameters and seven data points. This gives us 4 degrees of freedom for our fit. The

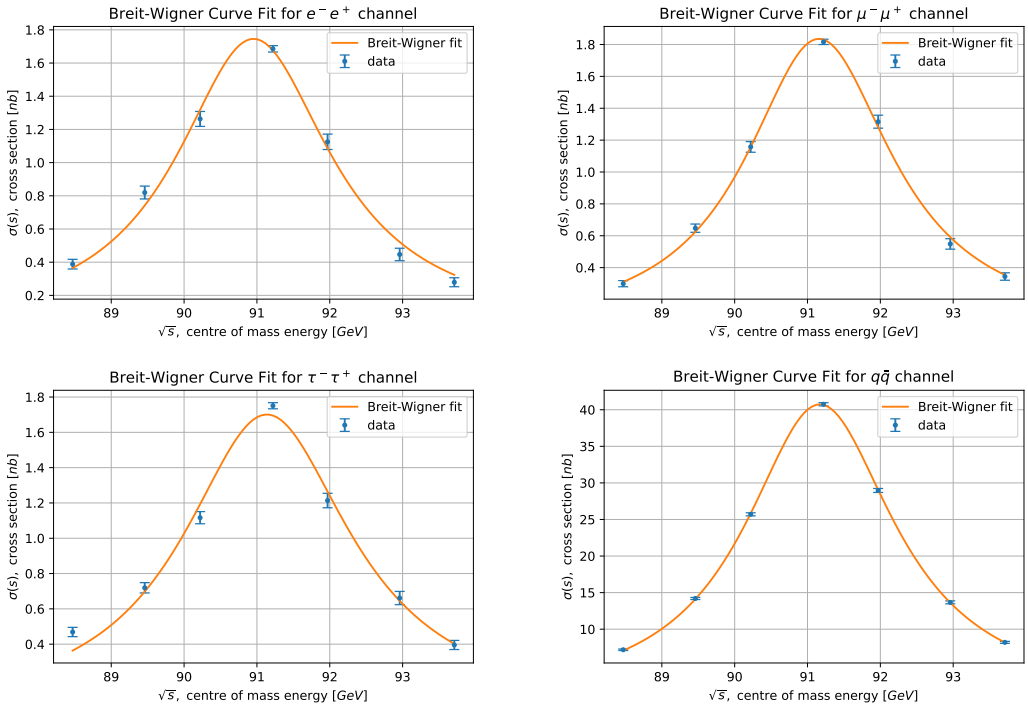

Figure 3.1: Breit-Wigner fit for the four different decay channels

Channel	M_Z [GeV]	Γ_Z [GeV]	$\Gamma_e\Gamma_f$ [GeV^2]	χ^2_{red}
e^-e^+	90.973 ± 0.047	2.591 ± 0.158	6.615×10^{-3} ± 6.29×10^{-4}	3.47
$\mu^-\mu^+$	91.117 ± 0.021	2.462 ± 0.060	6.306×10^{-3} ± 2.46×10^{-4}	1.10
$\tau^-\tau^+$	91.159 ± 0.058	2.825 ± 0.179	7.690×10^{-3} ± 7.85×10^{-4}	8.34
$q\bar{q}$	91.187 ± 0.004	2.515 ± 0.010	0.1460 ± 0.0009	0.58

Table 3.4: Fit parameters and reduced χ^2 values for the data

$\mu^-\mu^+$ fit gives the best reduced χ^2 value. The reduced χ^2 value for $q\bar{q}$ is less than 1, which implies that we are over-fitting the data or the error variances are overestimated. The reduced χ^2 value for e^-e^+ is greater than 1, which implies that we are under-fitting the data or the error variances are underestimated. Whereas, the reduced χ^2 value for $\tau^-\tau^+$ is much greater than 1, which implies that we don't have a good

fit[13]. But, none of the fits have a corresponding $p - value$ less than 0.05, which means they're not significant enough to be considered seriously different from previous literature results[14]. One major issue with using reduced χ^2 statistic test here is that we have only a limited number of points. Therefore, we don't have a lot of freedom to fit the data with. This ultimately results in a bad value, even though the fit is seemingly nice giving decent values for the parameters. If we had such a good data with more data points, we should obtain a better reduced χ^2 value. Our opinion is that the residuals give a better picture on whether we have a good fit, in our case. And all the residuals here are very small compared to the absolute values that we fit, which means that we have a decent fit for our data. For a better quantitative analysis of goodness of fit, we suggest methods like *bootstrapping*. Reduced χ^2 statistic test is not considered meaningful for limited number of points by some sources[15].
The fit parameters directly give us the values of mass of the Z^0 boson, M_Z and the decay width of the Z^0 boson, Γ_Z. The mean value of the quantities are,

$$\begin{aligned} M_Z &= 91.123 \pm 0.020 \text{ GeV} \\ \Gamma_Z &= 2.598 \pm 0.062 \text{ GeV}. \end{aligned} \tag{3.19}$$

The literature values are $M_Z = 91.1876 \pm 0.0021$ GeV and $\Gamma_Z = 2.4952 \pm 0.0023$ GeV [12]. The literature value for M_Z lies within 4σ of our calculated value, whereas the literature value for Γ_Z lies within 2σ of our calculated value. We also note that the literature value for M_Z lies within one standard deviation of the value obtained from the $q\bar{q}$ fit, which had the most counts. This hints us that we could improve our accuracy of the results by significantly increasing the number of events analysed.

3.2.7 Partial Width of Different Channels and Number of Light Neutrino Generations

The third fit parameter doesn't directly give us the partial decay width of different channels. It gives the product of the partial decay width of e^- mode and the partial decay width of f mode, the final state fermion in consideration. In the case of e^-e^+ channel, this reduces to Γ_e^2, which lets us calculate the partial decay width of the e^- mode. This can then be used to calculate the partial width of other channels. This is given in the table 3.5.
The literature values for Γ_f are taken from [12]. The literature values lie within one standard deviation

Channel	Γ_f [MeV]	Γ_f (lit.) [MeV]
e^-e^+	81.33 ± 5.47	83.91 ± 0.12
$\mu^-\mu^+$	77.53 ± 6.03	83.99 ± 0.18
$\tau^-\tau^+$	94.56 ± 11.55	84.08 ± 0.22
$q\bar{q}$	1795.52 ± 121.31	1744.4 ± 2.0

Table 3.5: Partial decay width of different channels and literature values

of the calculated partial width, which is impressive. But we also note that the precision of our results is not as good as the literature value precision. How precise the value of Γ_f is, ultimately depends on the precision of the cross section values, which can be improved only by observing more events.
With all the decay widths in hand, we can now determine the number of generations of light neutrinos. We use the value for Γ_ν from [5], which is $\Gamma_\nu = 167.6 MeV$. With this, we can calculate the number of neutrino generations using,

$$n_\nu = \frac{\Gamma_Z - \Gamma_e - \Gamma_\mu - \Gamma_\tau - \Gamma_q}{\Gamma_\nu}. \tag{3.20}$$

This gives the number of neutrino generations as,

$$n_\nu = 3.28 \pm 0.45. \tag{3.21}$$

This tells us that number of neutrino generations are 3. And within one standard deviation, our result absolutely excludes the possibility of fourth neutrino generation.

3.2.8 Discussion

References

[1] M. Thomson, *Modern particle physics* (Cambridge University Press, 2013).

[2] J. Erler and A. Freitas, *Electroweak Model and Constraints on New Physics*, English, Mar. 2018.

[3] S. K. Dooling, "Differential Cross Section Measurement of Drell-Yan Production and associated Jets with the CMS Experiment at the LHC", OA; Universität Hamburg, Diss., 2015, Dr. (Universität Hamburg, 2015), p. 242.

[4] D. J. Griffiths, *Introduction to elementary particles; 2nd rev. version*, Physics textbook (Wiley, New York, NY, 2008).

[5] Universität Bonn, *Instructions for E213: analysis of Z^0 decay.*

[6] P. Janot and S. Jadach, "Improved Bhabha cross section at LEP and the number of light neutrino species", Phys. Lett. B **803**, 13 tables, 4 figures, 135319. 12 p (2019).

[7] *Dark Matters:Creation from Annihilation*, `https://www.quantumdiaries.org/2014/11/13/dark-matters-creation-from-annihilation/`.

[8] G. Abbiendi et al. and T. Collaboration, "Precise determination of the Z resonance parameters at LEP: "Zedometry"", The European Physical Journal C - Particles and Fields **19**, 587–651 (2001).

[9] P. Zyla et al. (Particle Data Group), "Review of Particle Physics", PTEP **2020**, and 2021 update, 083C01 (2020).

[10] W. Feller, *An introduction to probability theory and its applications, volume 1*, en, 3rd ed., Wiley Series in Probability and Statistics (John Wiley & Sons, Jan. 1968).

[11] M. Lefebvre, R. K. Keeler, R. Sobie, and J. White, "Propagation of errors for matrix inversion", `10.1016/S0168-9002(00)00323-5` (1999).

[12] M. T. et al., "Review of particle physics", Physical Review D **98**, `10.1103/physrevd.98.030001` (2018).

[13] P. R. Bevington and D. K. Robinson, *Data reduction and error analysis for the physical sciences* (McGraw-Hill, New York, NY, Nov. 1969).

[14] *Critical Values of the Chi-Square Distribution*, `https://www.itl.nist.gov/div898/handbook/eda/section3/eda3674.htm`.

[15] R. Andrae, T. Schulze-Hartung, and P. Melchior, *Dos and don'ts of reduced chi-squared*, 2010.

Data

Table A.1: Event display analysis data for e^-e^+ channel(pure data).

EVENT	Ctrk(N)	Ctrk(Sump)	Ecal(SumE)	Hcal(SumE)
1	2	50.9	82.6	0
2	2	91.9	90	0
3	3	82.5	92.3	0
4	2	80.9	86.8	0
5	2	38.1	89.5	0
6	2	83.8	87.5	0
7	2	87.4	93.2	0
8	2	69.3	90.7	0
9	2	86.1	89.4	0.5
10	2	90.3	90.6	0
11	2	92.1	88.5	0.5
12	3	81.7	91.6	0
13	2	89.6	92.5	0
14	2	61.1	89.2	0
15	3	88.4	89.1	0
16	2	90.9	90.5	0.3
17	2	64.6	88.8	0
18	2	95.6	96.2	0
19	2	93	90.8	0
20	2	94.1	89.2	0

Table A.2: Event display analysis data for $\mu^-\mu^+$ channel(pure data).

EVENT	Ctrk(N)	Ctrk(Sump)	Ecal(SumE)	Hcal(SumE)
1	2	90.1	1.6	7
2	2	93	1.6	8.7
3	2	96.8	2	0
4	2	89.1	2.3	8.5
5	2	90.25	1.5	7.2
6	2	91.8	1.8	4.3
7	2	86.3	3.7	3.3
8	2	99.2	1.3	2.9
9	2	88.2	1.6	3
10	2	90.9	1.3	6.7
11	2	95.6	2.5	6.1
12	2	75.3	3.1	6.8
13	2	85.2	5.8	4.4
14	2	98.6	3.6	5.7
15	2	86.8	1.9	7.9
16	2	98	1.9	2
17	2	108.3	2	8.5
18	2	92.4	3.6	6.7
19	2	92	1.9	22.6
20	2	92.6	3.6	5.7

Table A.3: Event display analysis data for $\tau^-\tau^+$ channel(pure data).

EVENT	Ctrk(N)	Ctrk(Sump)	Ecal(SumE)	Hcal(SumE)
1	5	74	51.1	10.2
2	2	46.5	17.3	8.2
3	2	30.8	1.6	6.3
4	2	29.5	10.2	4.1
5	2	33.1	1.5	10.6
6	2	24.4	12.4	11.7
7	4	36	16.1	5.7
8	2	41.3	11.1	20
9	2	49.7	5.2	20.3
10	2	33.4	23.6	6.9
11	2	14.1	3.3	6.3
12	2	19.7	15.9	3.8
13	2	26.8	16.5	3.4
14	5	23.4	27	17.1
15	2	23.8	29.4	3.6
16	2	39	18.9	4.4
17	2	24.1	46.5	7.3
18	5	38.5	28.5	0
19	2	35.3	51.8	2.3
20	2	17.8	2.5	5

Table A.4: Event display analysis data for $q\bar{q}$ channel(pure data).

EVENT	Ctrk(N)	Ctrk(Sump)	Ecal(SumE)	Hcal(SumE)
1	15	37.7	37	14.1
2	17	39.2	66.8	9.9
3	46	64.6	53	13
4	36	45.3	53.2	7.7
5	41	59.9	53.2	13.8
6	9	21.9	65.2	8.8
7	16	55.9	50.4	24.3
8	30	38.1	68.3	13.8
9	22	34.4	75.5	6.2
10	36	51.2	62.3	5.5
11	23	63.1	56	17.2
12	23	59	60.6	8.5
13	26	62.2	67.2	20.4
14	30	43.3	71.7	4.3
15	40	47.8	61.4	5.7
16	19	67.9	52.1	10.6
17	14	52.1	61	4.4
18	29	82.6	53.8	16.4

Table A.5: Event display analysis for mixed data

EVENT	Ctrk(N)	Ctrk(Sump)	Ecal(SumE)	Hcal(SumE)	Channel
1	19	39.5	44.3	15.6	$q\bar{q}$
2	36	42.8	57.1	12.5	$q\bar{q}$
3	2	95.7	93.4	0	e^-e^+
4	2	90.8	1.4	4.1	$\mu^-\mu^+$
5	4	36.5	35.8	10.8	$\tau^-\tau^+$
6	2	97	2.2	8.9	$\mu^-\mu^+$
7	68	42.9	48.5	6.2	$q\bar{q}$
8	5	35	40.8	3.3	$\tau^-\tau^+$
9	21	75.8	45.8	21	$q\bar{q}$
10	2	95.2	1.3	7.9	$\mu^-\mu^+$
11	2	22.7	34.4	0	$\tau^-\tau^+$
12	4	44.3	37.8	2.6	$\tau^-\tau^+$
13	21	53.1	36.2	22.9	$q\bar{q}$
14	2	89.5	92	0	e^-e^+
15	2	89.1	89.7	0	e^-e^+
16	2	4.1	4.4	0	$\tau^-\tau^+$
17	2	87.8	1.4	4.3	$\mu^-\mu^+$
18	2	75.3	90	0	e^-e^+
19	2	93.7	1.6	6.8	$\mu^-\mu^+$
20	2	67.1	93.6	0	e^-e^+

Table A.6: Observed event numbers and actual events numbers for different $\sqrt{s}$ values.

$\sqrt{s}$ [GeV]	e^-e^+	$\mu^-\mu^+$	$\tau^-\tau^+$	$q\bar{q}$
	N_{obs}			
88.47	106	120	251	3281
89.46	261	304	425	7413
90.22	415	591	693	14709
91.22	4839	8581	10178	221068
91.97	393	767	863	18728
92.96	150	296	427	8100
93.71	178	339	459	8635
	N_{actual}			
88.47	202 ± 20	141 ± 13	256 ± 18	3508 ± 61
89.46	496 ± 31	358 ± 21	416 ± 23	7927 ± 92
90.22	789 ± 39	697 ± 29	661 ± 30	15729 ± 130
91.22	920 ± 137	1023 ± 111	971 ± 120	236399 ± 541
91.97	747 ± 38	904 ± 33	820 ± 33	20026 ± 147
92.96	285 ± 23	349 ± 20	419 ± 23	8662 ± 96
93.71	338 ± 25	400 ± 22	448 ± 24	9234 ± 100

Table A.7: Integrated luminosity values for *data6.root* and radiative and A_{FB} corrections for different $\sqrt{s}$ values[5].

$\sqrt{s}$ [GeV]	$\int \mathcal{L}dt[\text{nb}]^{-1}$	Rad. Correction [nb]		A_{FB} Correction
		Hadronic	Leptonic	
88.47	675.9 ± 5.7	+2.0	+0.09	0.021512
89.46	800.8 ± 6.6	+4.3	+0.20	0.019262
90.22	873.7 ± 7.1	+7.7	+0.36	0.016713
91.22	7893.5 ± 54.3	+10.8	+0.52	0.018293
91.97	825.3 ± 6.9	+4.7	+0.22	0.030286
92.96	624.6 ± 5.5	-0.2	-0.01	0.062196
93.71	942.2 ± 7.7	-1.6	-0.08	0.093850

Plots

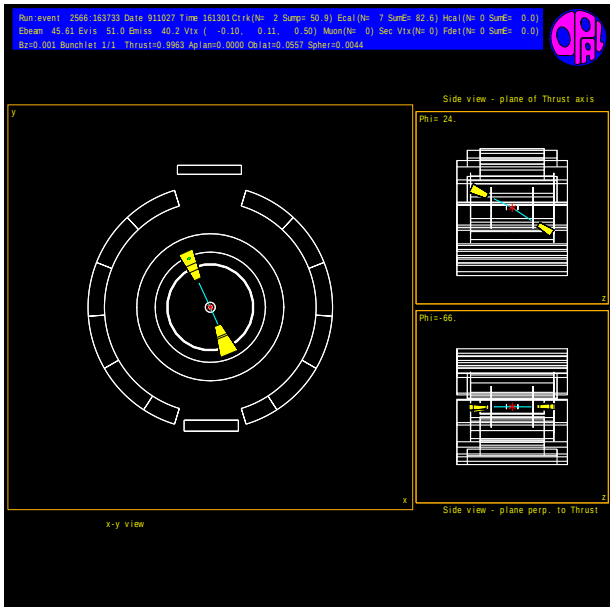

Figure B.1: Event display of e^-e^+-channel sample

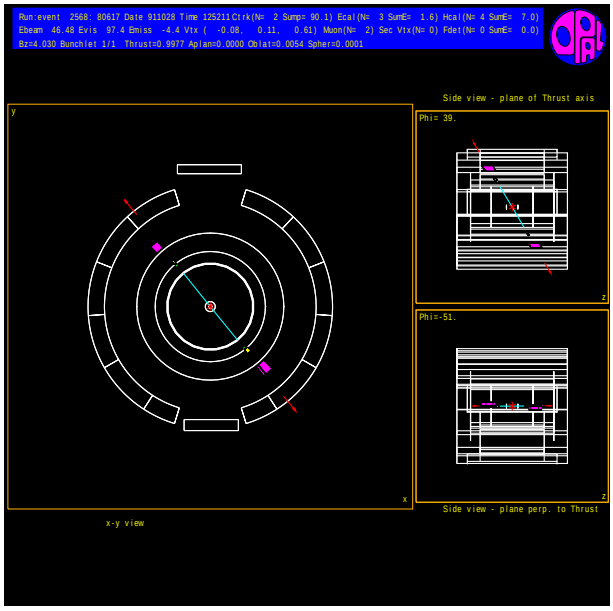

Figure B.2: Event display of $\mu^-\mu^+$-channel sample

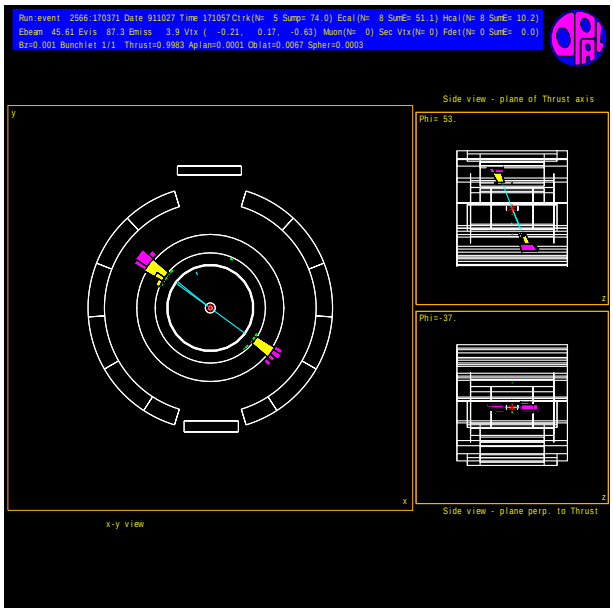

Figure B.3: Event display of $\tau^-\tau^+$-channel sample

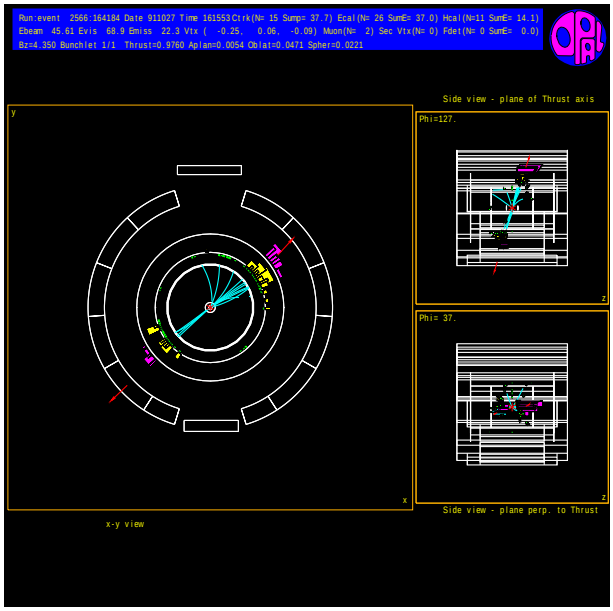

Figure B.4: Event display of $q\bar{q}$-channel sample

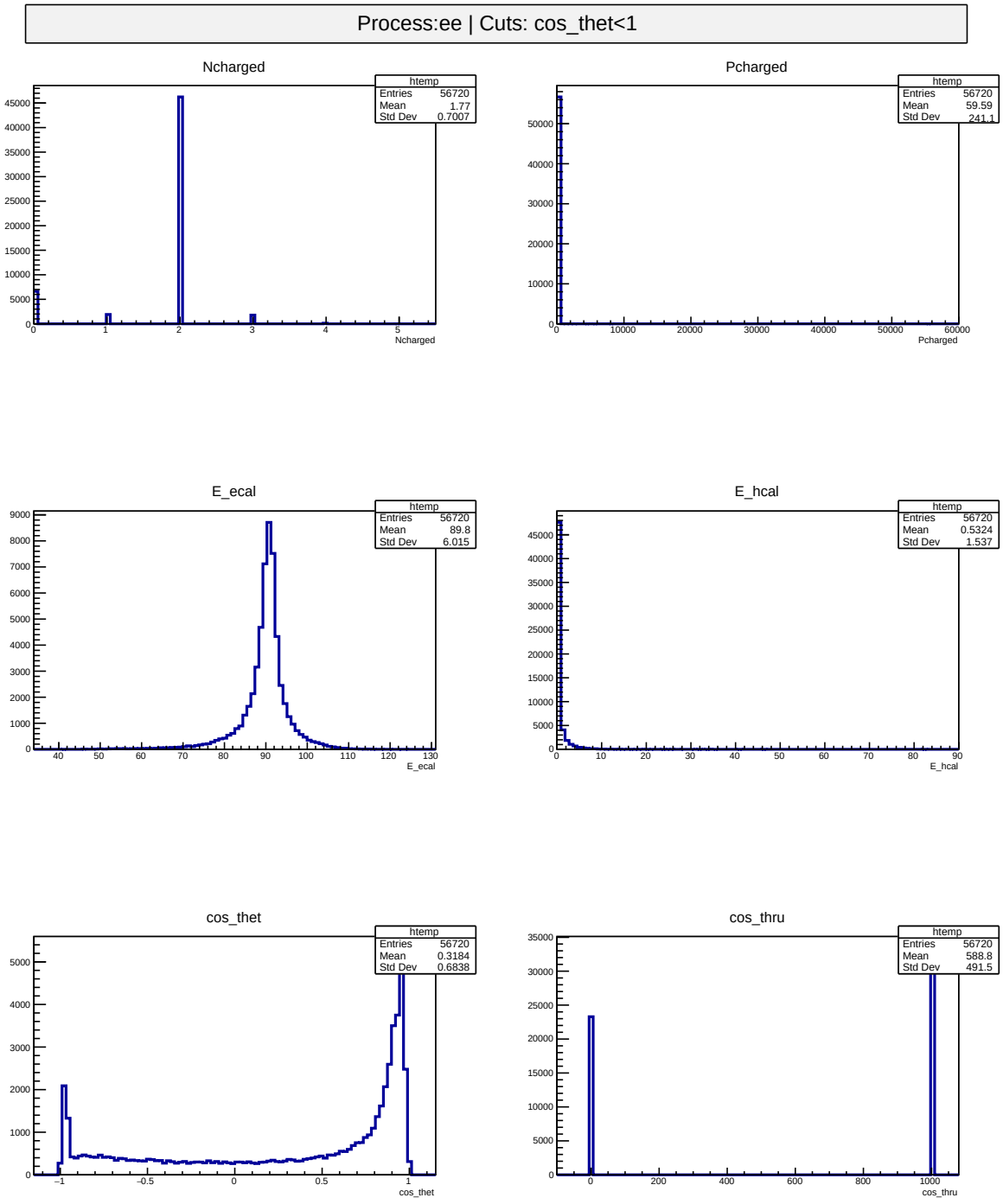

Figure B.5: Global cuts applied to $e^{-}e^{+}$ MC

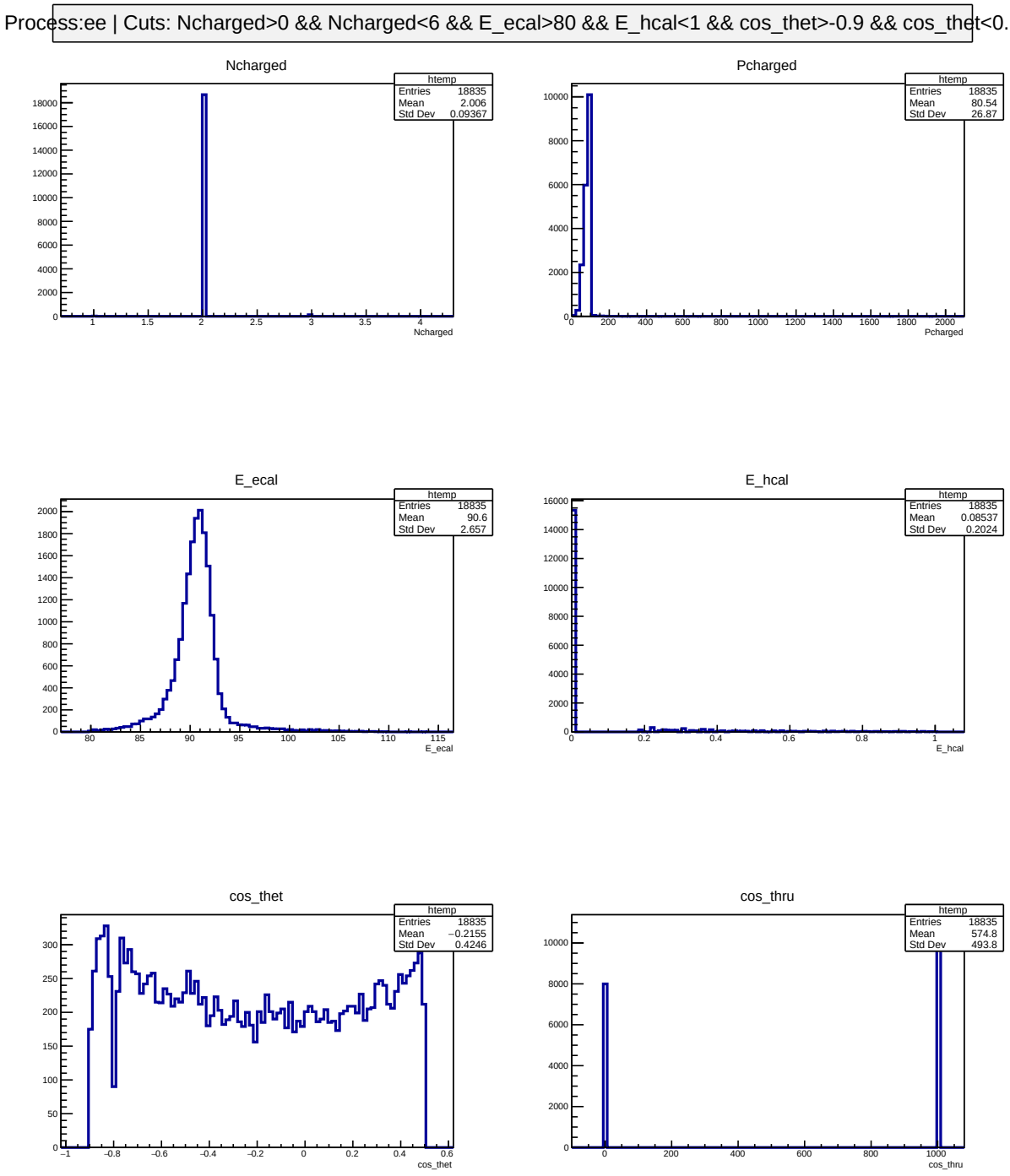

Figure B.6: e^-e^+ cuts applied to e^-e^+ MC

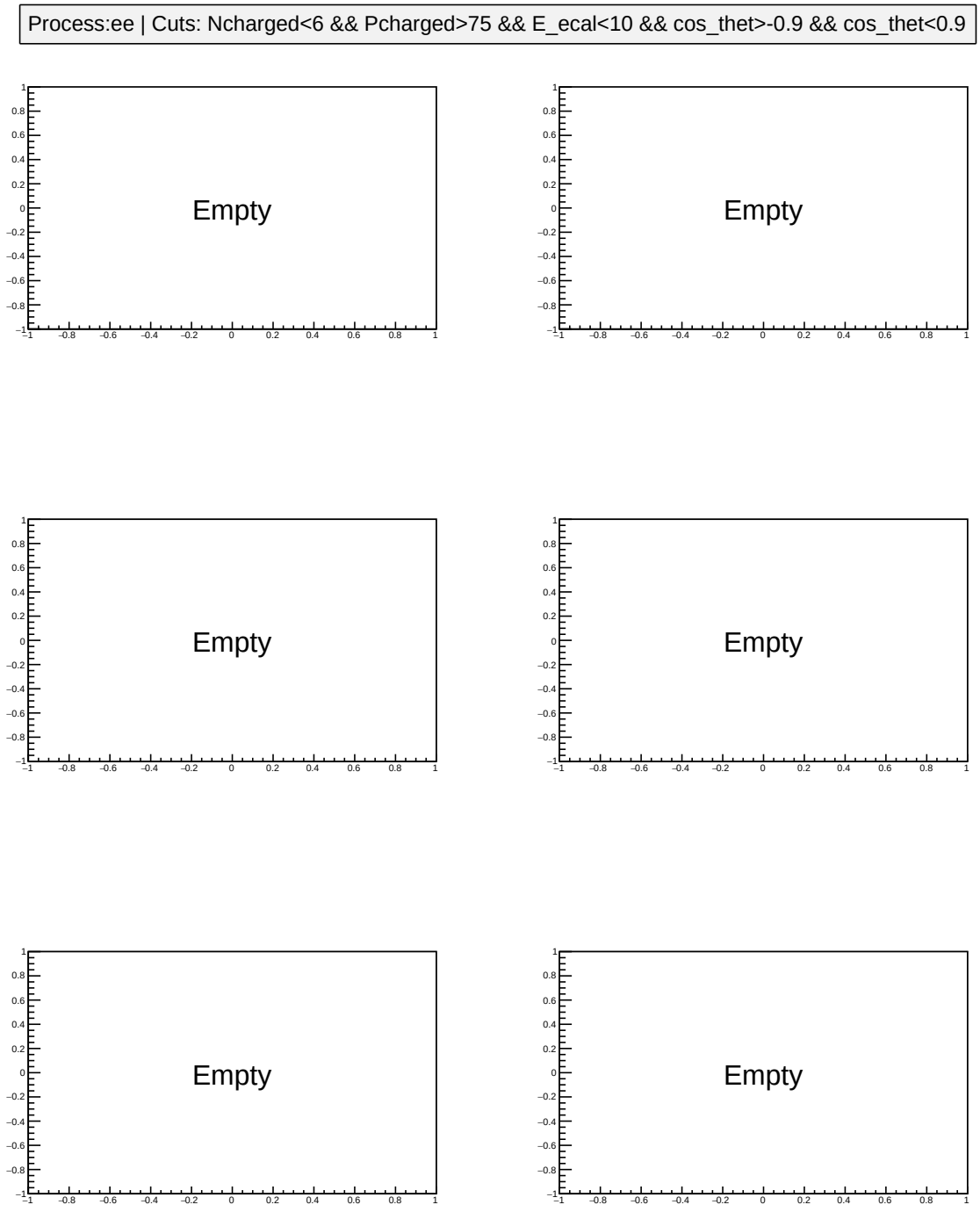

Figure B.7: $\mu^-\mu^+$ cuts applied to e^-e^+ MC

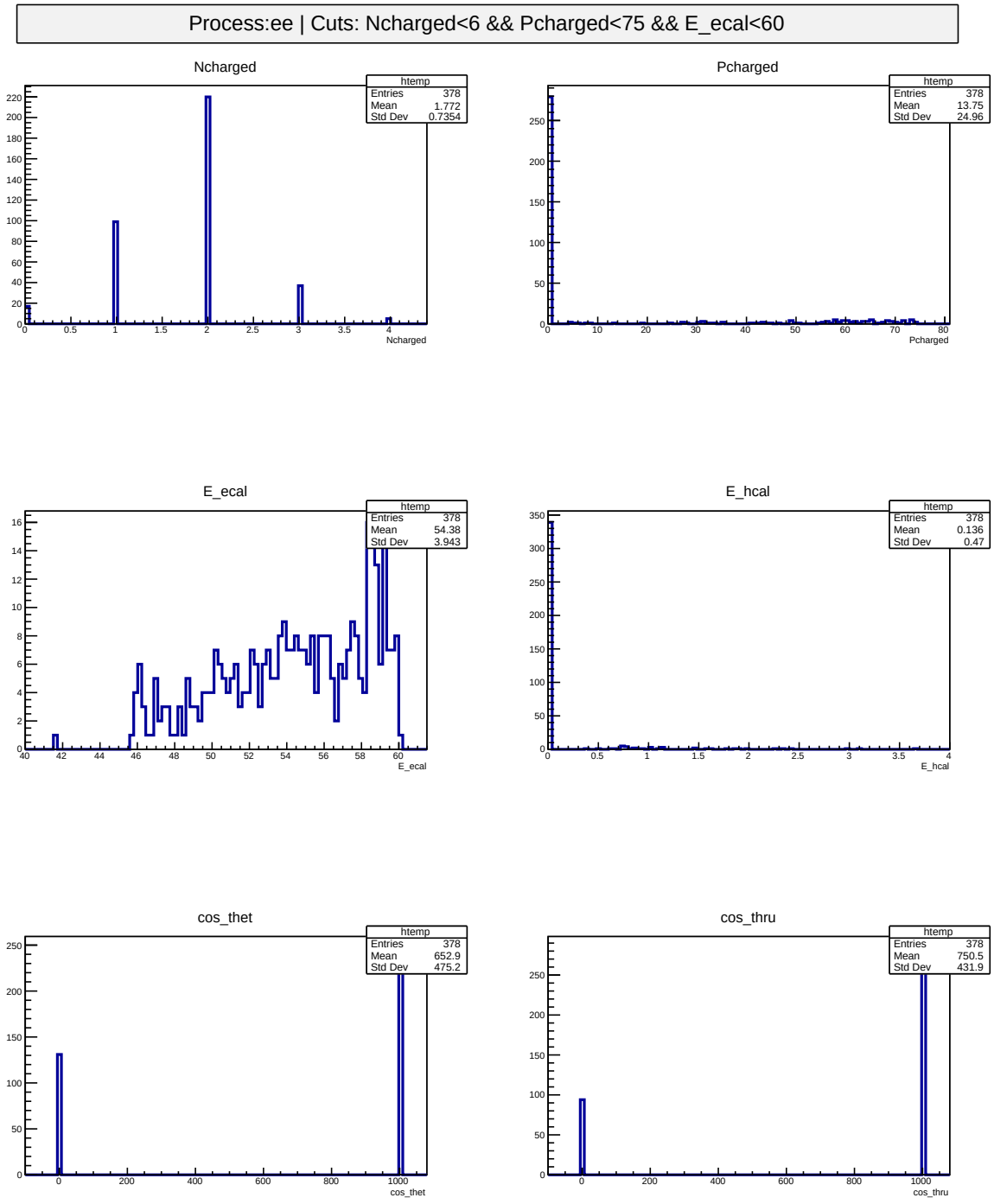

Figure B.8: $\tau^-\tau^+$ cuts applied to e^-e^+ MC

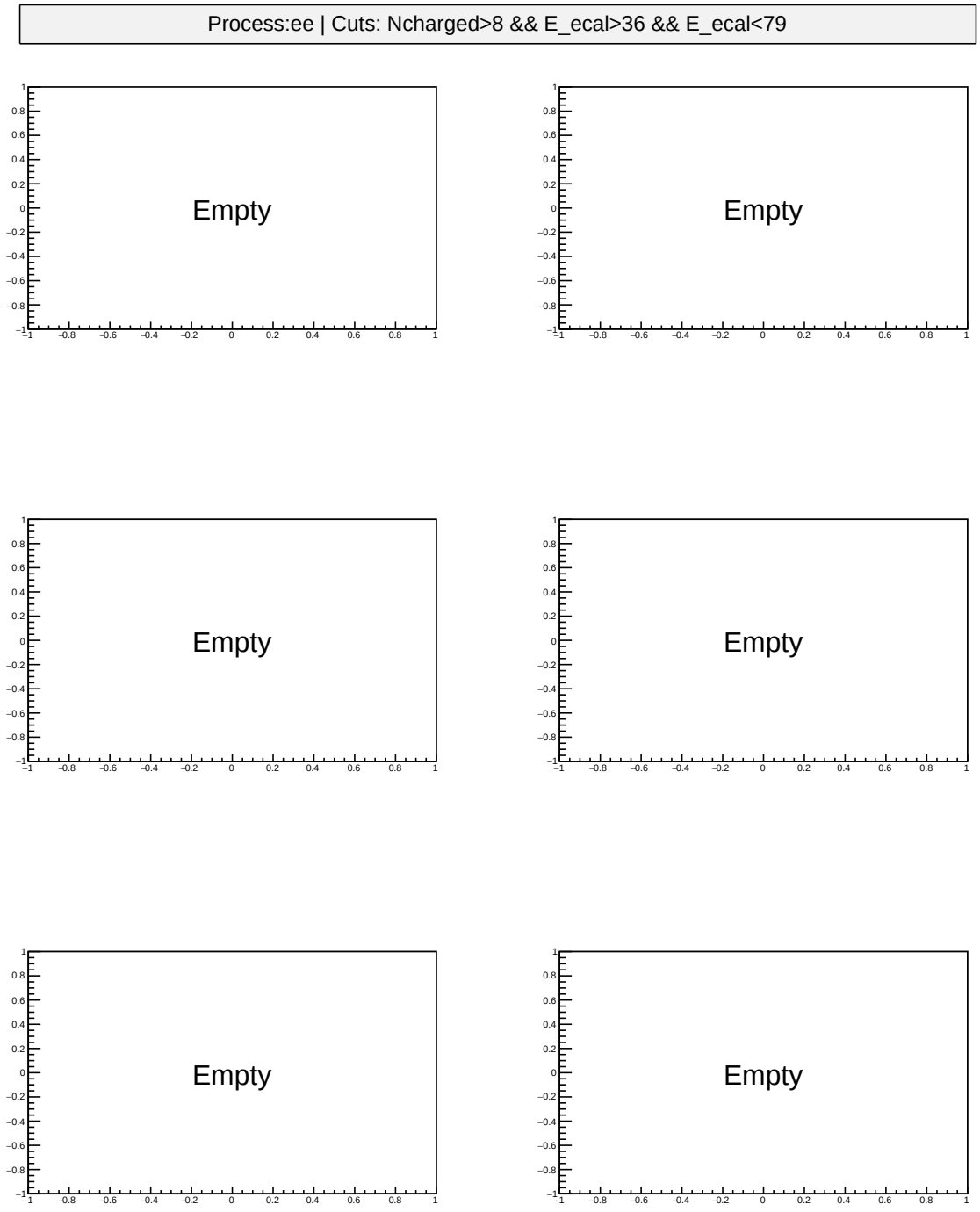

Figure B.9: $q\bar{q}$ cuts applied to e^-e^+ MC